Synthesis of Sulfur-doped Calcium Carbonate Nanocomposite Semiconductor Derived from Chicken Eggshell Powder

Rodhiansyah Djayasinga[1], Sutopo Hadi[2], Sumardi Sumardi[3], Wasinton Simanjuntak[4], Mimi Sugiarti [5], and Rudy Tahan Mangapul Situmeang[6]

[1]Doctoral Program of Mathematics and Natural Science, University of Lampung Jl. Prof. Dr. Sumantri Brojonegoro No. 1 Bandar Lampung, 35145, Indonesia
[2,4,6]Department of Chemistry, Faculty of Mathematics and Natural Sciences, University of Lampung, Bandar Lampung 35145, Indonesia
[5]Department of Medical Laboratory Technology, Tanjungkarang Health Polytechnic, Lampung-35145, Indonesia
[3]Department of Biology, Faculty of Mathematics and Natural Sciences, University of Lampung, Bandar Lampung 35145, Indonesia
rudy.tahan@fmipa.unila.ac.id

Abstract. This study successfully leveraged chicken eggshells to fabricate sulfur-doped calcium carbonate(S/$CaCO_3$) nanocomposite semiconductor materials. The synthesis process employed the sol-gel method through two eco-friendly steps. The first stage is the synthesis of calcium oxide nanoparticle precursors (CaO Nps) from chicken egg shell powder waste. Subsequently, the CaO Nps were dispersed in a methanol-glycerol mixture, and thiourea was added as the sulfur source. Characterization techniques, including Thermogravimetric-Differential Thermal Analysis (TG-DTA), Fourier Transform Infrared spectroscopy (FTIR), X-Ray Diffraction (XRD), and Ultraviolet-Visible Diffuse Reflectance Spectroscopy (DRS-UV-Vis), were employed to analyze the synthesized material. The results showed that a semiconductor S/$CaCO_3$ nanocomposite with a size of 22.72 nm, and the bandgap energy decreases from the CaO Nps precursor by 5.67 eV to 1.82 eV for the S/$CaCO_3$ nanocomposite. The formation of the S/$CaCO_3$ nanocomposite was confirmed by the overlapping crystal phases at 2θ between $CaCO_3$ (vaterite), and sulfur, as well as the FTIR analysis revealing a characteristic S=O stretching at 1148 Cm^{-1}. The obtained percentage of the S/$CaCO_3$ nanocomposite was 57.09%, indicating that further optimization is possible to achieve a higher product yield.

Keywords: CaO nanoparticles, Chicken eggshell powder waste, Semiconductor, S/$CaCO_3$ nanocomposite, Thiourea.

S. Hadi et al. (eds.), *Proceedings of the 5th International Conference on Applied Sciences, Mathematics, and Informatics (ICASMI 2024)*, Advances in Physics Research 13,
https://doi.org/10.2991/978-94-6463-730-4_15

1 Introduction

Semiconductor materials play a crucial role in the development of modern technology, as they are the fundamental materials used in the fabrication of electronic components such as batteries, microprocessors, memory devices, and sensors[1-2]. These components are the brain and primary driver of various electronic devices commonly used by the world's population, such as smartphones, computers, and electric vehicles[3]. Various methods and raw materials have been extensively developed for the production of semiconductor materials, as has been done by Kuznetsova [4] who has researched the synthesis of hybrid conductive polymer nanocomposites, particularly for biomedical applications such as biosensors; the synthesis of chitosan-based nanocomposites for environmental applications, but also exploring the properties and potential use of electronic materials due to their multifunctional nature[5]; graphene nanocomposites, discussing their potential in high-performance transistors, sensors, and solar cells[6]; exploration of calcium carbonate ($CaCO_3$) as a material in optoelectronic devices[7]; calcium carbonate can be used as a filler in polymer nanocomposites or other materials to improve mechanical, thermal, or even optical properties, while other semiconductor materials are responsible for their electronic properties[8].

Calcium carbonate which is fundamentally an insulating material, can have its properties modified when combined with other semiconductor materials or in the form of a nanocomposite[9]. Several studies have shown that the shift in the energy absorption threshold is crucial for effective utilization of sunlight for electron transfer, as impurities such as C, S, or N are often used to modify the electronic structure and optical properties of many materials[10-11]. Specifically, sulfur doping has received more attention due to its high electronegativity, such as research on sulfur-doped graphitic carbon nitride (g-C_3N_4) nanomaterials. The obtained bandgap energy was reduced by 0.7 eV, resulting in a value of 2.7 eV, and the material synthesis used a thermal polymerization method with a precursor mixture containing melamine and sulfur-containing compounds. The mixture was then heated at high temperatures under an atmosphere. This process resulted in sulfur doping and methylation of the (g-C_3N_4) nanosheets, which enhanced their photocatalytic properties[12-13].

Additionally, investigated that sulfur doping in MoO_3 was able to shift the bandgap from 2.68 eV to 2.57 eV. This study highlighted how the interaction of sulfur with oxygen vacancies significantly enhanced the optoelectronic properties. Sulfur sources were used in combination with molybdenum trioxide. The hydrothermal process enabled the incorporation of sulfur atoms into the MoO_3 structure, forming Mo-S bonds[14]. Based on previous literature information, the researchers identified that there has been no research on the synthesis of semiconductor materials using sulfur-doped calcium carbonate from chicken eggshells waste.

2 Material and methods

This study was carried out at the Chemistry Laboratory of Tanjungkarang Health Polytechnic, Department of Medical Laboratory Technology, during the period from

July to September 2024. The materials used were chicken eggshells sourced from domestic waste, glyserol, thiourea, methanol, NaOH, HCl, $AgNO_3$ from Merck. Istrumentation used; Muffle furnace (Labomiz scientific), Analitical balance (BEL Model MW 333i type MWnn3i-M), sieve 100 mesh, Fourier Transform Infra-Red (Agilent Technologies Carry 630), X-Ray Diffraction Shimadzu XRD-700, Termo-gravimetric analyzer (NEXTA STA Hitachi STA200RV).

2.1 Synthesis of CaO nanoparticles from chicken eggshell waste

The chicken eggshells were ground into a fine powder using a porcelain mortar and sieved through a 100-mesh screen. Next, 12.5 g of the eggshell powder were mixed with 250 mL of 0.1 M hydrochloric acid solution, and the formed foam was discarded. The mixture was then centrifuged at 2000 rpm for 10 minutes, and the sediment and solution were separated. This process was repeated twice. The separated solution was then slowly added dropwise using a burette with 250 mL of 0.1 M sodium hydroxide solution until a white mixture was formed. The white mixture was allowed to settle for 24 hours, and then decanted. The sediment was washed twice used distilled water. The clear solution was tested with a few drops of 0.1 M silver nitrate solution, and the formation of a brown color indicated that the washing with hot distilled water was complete. The decantation was continued until only the sediment remained. The sediment was then placed in a porcelain dish and dried in an oven at 80 ℃ until dry. After drying, the sediment was calcined at a temperature of 900 ℃ for 1 hour[15].

2.2 Synthesis of S/$CaCO_3$ nanocomposites

In this study, the sol-gel method was modified from the procedure described by Cheng [16], Specifically, 35 mL of glycerol was combined with 200 mL of methanol and magnetically stirred at 350 rpm. Subsequently, 2 g of CaO nanoparticles were added and stirred at the same speed for 30 minutes. Afterward, 1 g of thiourea was incorporated, and the mixture was magnetically stirred for 1 hour. The temperature was then raised to 80 ℃, and once the volume reached 100 mL, the stirring was halted. Finally, the mixture was dried in an oven at 90 ℃ for 11 hours and then calcined at 450 ℃ for 15 hours.[17-18].

3 Result and discussion

The thermogravimetric analysis results depicted in Fig 1 offer insights into the mass changes observed. Three distinct mass decreases were noted: from 26 ℃ to 384.7 ℃, a 3.51% reduction attributed to the evaporation of physically adsorbed water; from 384.7 ℃ to 480.3 ℃, a 20.29% reduction due to the transformation of $Ca(OH)_2$ into CaO; and from 480.3 ℃ to 684.6 ℃, a 26.52% weight reduction resulting from the decomposition of $CaCO_3$ into CaO[19-20]. The DTA analysis results reveal the presence of two endothermic peaks, one at 89.0 ℃ and the other at 445.6 ℃. Additionally, the DTA analysis provides information on the temperature difference between the

sample and the reference material, which is 998 μV·s/mg. Moreover, the DTA plot indicates that the sample's maximum mass change rate took place at 441.5 ℃, with a rate of 0.209 μg/min.

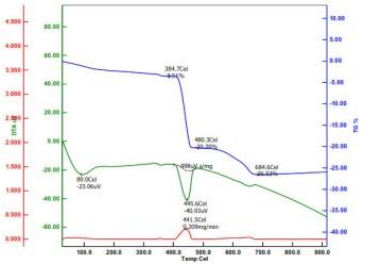

Fig. 1. TG-DTA analysis results of $Ca(OH)_2$ precursor

Fig 2 depicts the calcium oxide nanoparticles produced using a modified sol-gel synthesis method. When hydrochloric acid solution was introduced, a hydrolysis reaction occurred between the $CaCO_3$ in the eggshell powder and HCl, generating a $CaCl_2$ sol, water, and CO_2 gas that manifested as foam. Subsequently, the $CaCl_2$ sol was combined with a sodium hydroxide solution, leading to the formation of a $Ca(OH)_2$ precursor gel due to a condensation reaction, which consequently resulted in the creation of an inorganic network from small particles weakly bound by covalent forces[21].

Fig. 2. CaO nanoparticles products

The generated foam was not utilized in the subsequent steps, as it could have interfered with the formation of the $Ca(OH)_2$ precursor and the production of NaCl when sodium hydroxide was added to the calcium chloride solution. The washing with hot deionized water aimed to remove impurities such as chloride and sodium ions, as well as other organic compounds. Additionally, the test with silver nitrate solution was conducted to verify the absence of chloride ions, which would be indicated by the formation of a brown precipitate, a compound of silver hydroxide.

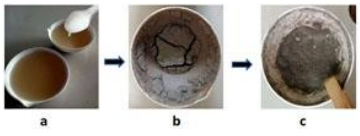

Fig. 3. Color changes observed during the synthesis of $S/CaCO_3$

The use of glycerol and methanol during synthesis aimed to provide a dispersive medium for CaO nanoparticles, along with thiourea. Fig 3a depicts the orange-colored, gel-like $S/CaCO_3$ precursor formed after drying in the oven. Figure 3b shows

the dark brown $S/CaCO_3$ nanocomposite product following calcination, before grinding. Additionally,Fig 3c presents the slightly reddish-brown powdered $S/CaCO_3$ product after grinding.

Fig. 4 reveals that the presence of the O-H stretching vibration peak at 3642 Cm^{-1} suggests the adsorption of water molecules on the surface of the crystal phase [22]. The wavenumbers 2994 Cm^{-1} and 2893 Cm^{-1} indicate the presence of asymmetric and symmetric C-H stretching vibrations, respectively[23]. The O=C=O stretching functional group is identified at 2395 Cm^{-1} [24]. Next, at the wavenumber of 1409 Cm^{-1}, it represents the C-H bending vibration[25]. S=O stretching was observed at 1148 Cm^{-1} [26-27].The wavenumbers at 1250 Cm^{-1}, 1075 Cm^{-1}, and 746 Cm^{-1} suggest the presence of the C-O stretching vibration . The FTIR spectrum indicated the presence of CaO stretching vibrations at wavenumbers of 878 Cm-1, 872 Cm^{-1}, and 713 Cm^{-1}, which was further corroborated by peaks at 688 Cm^{-1}, and 677 Cm^{-1} [28]

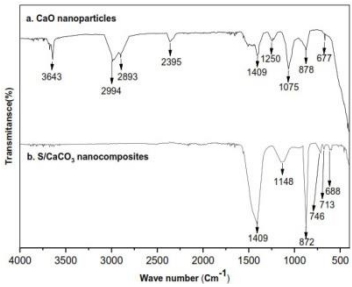

Fig. 4. Comparison FTIR analysis of CaO NPs, and S/CaCO3 nanocomposites

According to the XRD analysis conducted with the Match! Crystal Impact software version 3.15 build 247 for Windows 32-bit[29], by comparing the XRD patterns with the CIF-9006694 reference data. The XRD analysis data was processed using OriginLab 64-bit software to generate Fig. 5[30]. The peaks labeled A at 2θ (°) of; 32.19° (111) :37.33° (002): 53.83° (022) indicate the presence of the crystalline form of CaO. The 2θ (°) peaks observed are consistent with the findings reported in earlier studies[31].

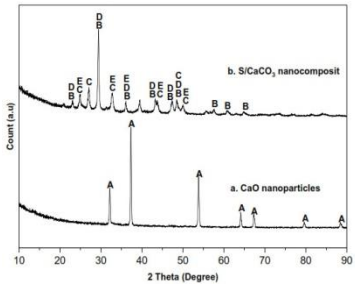

Fig. 5. Qualitative XRD analysis of CaO NPs, and $S/CaCO_3$ nanocomposite

The calcium carbonate crystal phase obtained from the synthesis was 62.49% $CaCO_3$ crystal phase (consisting of calcite, vaterite, magnesium calcite), and 37.51% sulfur. The peaks labeled C in Fig. 5 correspond to the crystalline $CaCO_3$ phase (vaterite), which was identified by comparing the data to the X-ray diffraction pattern with the CIF reference number CIF-amcsd-0009279[32]. These peaks indicate the diffraction angles at which the $CaCO_3$ (vaterite) phase is observed 2θ (°) ; 24.86° (010); 27.03° (011); 32.75° (012); 50.02° (014). Additionally, the crystalline phase of sulfur, denoted by label E, was also detected at 2θ (°); 24.90° (110); 32.77° (111); 35.90° (021), 50.03° (112) through analysis of the X-ray diffraction pattern with CIF reference number CIF-7214217[33]. The XRD analysis revealed an overlap between several crystalline phases, including the vaterite form of calcium carbonate (peaks 2θ labeled C), and the crystalline sulfur phase (peaks 2θ labeled E), as evident from Fig. 5. The overlap of these two crystalline phases confirms the formation of the S/$CaCO_3$ nanocomposite.

The ionic radius of S^{2-} is 0.18 nm, while O^{2-} is smaller, with a radius of 0.14 nm. This size disparity can disrupt the crystal structure of $CaCO_3$ when sulfur replaces oxygen, leading to more vacancies and crystal defects. Oxygen vacancies refer to the absence of oxygen atoms in the $CaCO_3$ crystal lattice. When sulfur takes the place of oxygen, these vacancies are likely to develop because sulfur does not fit well into the original oxygen position due to the size difference[34].

Oxygen is more electronegative than sulfur, meaning it attracts electrons more strongly in a chemical bond. This significant difference in electronegativity between sulfur and oxygen is relevant to how sulfur interacts with and substitutes for oxygen atoms in the $CaCO_3$ crystal lattice. Furthermore, the FTIR analysis detected the presence of S=O stretching at 1148 Cm^{-1}, supporting the formation of the S/$CaCO_3$ nanocomposite[35].

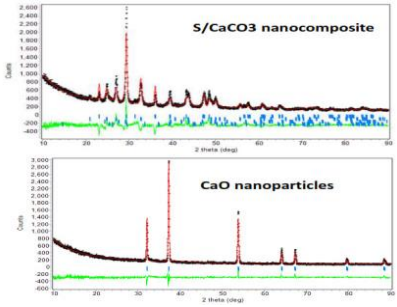

Fig. 6. Quantitative XRD analysis of CaO NPs, and S/$CaCO_3$ nanocomposite

Quantitative XRD analysis was performed to investigate the CaO crystal phase and S/$CaCO_3$ nanocomposite using the Rietica version 4.0 Rietveld analysis software[36]. The analysis compares the diffraction patterns of the CaO nanoparticle crystal phase and the S/$CaCO_3$ crystal phase, as depicted in Fig 6. The analysis of the CaO crystal phase yielded a Goodness of Fit value of 1.67, which satisfies the ideal criterion of being less than 4[37].

The calcium oxide crystal phase exhibits a cubic lattice structure with a cell parameter of a = 4.81310 Å, which correspond to the angles of ($\alpha = \beta = \gamma = 90$ °), The unit cell volume is 111.500267, and number of formulas per unit cell (Z) = 4. The atomic positions of the Ca and oxygen atoms is (x = 0 (Ca), x = 0.5 (O); y = 0 (Ca), y = 0.5 (O); z = 0 (Ca), z = 0.5 (O). The Goodness of Fit value for the S/$CaCO_3$ nanocomposite is 3.587. 7, weight percentage of phase $CaCO_3$ (vaterite) is 19.58%, and sulfur is 37.51%. The $CaCO_3$ (vaterite) crystal phase lattice is hexagonal with cell parameters (a = 4.14020 Å, c = 8.47490 Å), cell angles (α = β = 90 °, γ = 120 °), cell volume of 125.81, number of formulas per unit cell (Z) = 1, as well as the atomic positions of Ca, C, O, and O (x = 0 (Ca), x = 0.33788 (C), x = 22035 (O), dan x = 38000 (O); y = 0 (Ca), y = 0.75581 (C), y = 0.39463 (O), y = 64216 (O); z = 0 (Ca), z = 0.25000 (C), z = 25000 (O), z = 0.10767 (O).

Next are the characteristics of the sulfur crystal phase, namely trigonal (hexagonal) with cell parameters (a = 7.00220 Å, c = 3.94150 Å), cell angle (α = β = 90°, γ = 120°), cell volume = 167.360947, number of formulas per unit cell (Z) = 1. S atom position (x = 0.70420 (S), x = 0.76043 (S); y = 0.33764 (S), y = 0 (S); z = 0 .94273 (S), z = 0.16667 (S). Using the Debye-Scherrer formula, and the full width at half maximum value of 0.28 at 2θ (°) 37.33°, the size of the CaO nanoparticles was calculated to be 29.97 nm. Similarly, the S/$CaCO_3$ crystal phase has a FWHM value of 0.36 at 2θ (°) = 27.04°, corresponding to a particle size of 22.72 nm. Finally, the combined weight percentage of the vaterite phase and sulfur was determined to be 57.09%, indicating the proportion of the S/$CaCO_3$ nanocomposite.

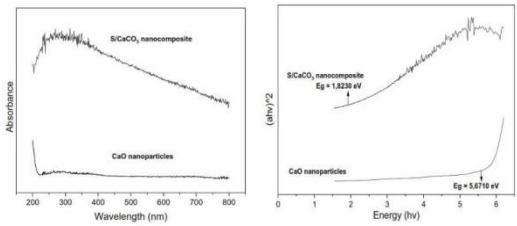

Fig. 7. Comparison of UV-Vis, and bandgap of CaO NPs, S/$CaCO_3$ nanocomposite

The data from Figure 7a shows the UV-Visible absorbance spectrum, which exhibits a peak absorption at 369.90 nm. Additionally, Fig 7b presents the calculated band gap energy value obtained using the Tauc plot method[38]. The results showed a band gap energy of 5.67 eV for the CaO nanoparticles, whereas the S/$CaCO_3$ nanocomposite exhibited a lower bandgap energy of 1.82 eV (r^2= 0.9907). The decrease in bandgap energy is facilitated by the presence of oxygen vacancies in the vaterite crystal structure, which are then occupied by sulfur atoms. However, the sulfur atoms do not occupy the same positions as the previous oxygen atoms, resulting in the formation of crystal defects. This alteration leads to a shift in the absorption energy threshold from the valence band to the conduction band [35]. The disparity between the two bandgap energy values suggests that the CaO nanoparticles derived from chicken eggshell powder possess the characteristics of an insulating material, whereas

the synthesized $S/CaCO_3$ nanocomposite exhibits the properties of a semiconductor material[39].

4 Conclusion

In summary, this study successfully synthesized sulfur-doped calcium carbonate ($S/CaCO_3$) nanocomposite semiconductor materials using the sol-gel method. The precursor materials were CaO NPs derived from chicken eggshell powder, and thiourea was used as the sulfur source. XRD analysis confirmed the formation of the $S/CaCO_3$ nanocomposite crystalline phase, characterized by the overlapping of the $CaCO_3$ (vaterite), and sulfur crystalline peaks. FTIR analysis at 1148 Cm^{-1} indicated the presence of S=O bonds. UV-Vis spectroscopy showed an absorption peak at 369.9 nm and a bandgap of 1.82 eV. The average crystal size of the $S/CaCO_3$ nanocomposite, calculated using the Debye-Scherrer equation, was 22.72 nm, with a yield percentage of 57.09%.

Acknowledgments. The researchers extend their sincere gratitude to the Ministry of Health of the Republic of Indonesia, which through Decree Number HK.02.03/F/2322/2023 of the Director General of Health Resources, provided the funding and opportunity to carry out this research. Additionally, the researchers also appreciate the support from the Faculty of Mathematics and Natural Sciences at the University of Lampung, which facilitated the completion of this study.

Disclosure of Interests. The authors have no competing interests

References

1. Yu, Y., Hu, S.: The applications of semiconductor materials in air batteries. Chinese Chem. Lett. **32**, 3277–3287 (2021)
2. Fantini, P., Servalli, G., Tessariol, P.: Semiconductor Memory Technologies. Presented at the (2023)
3. Qiu, Z., Shen, X., Zhao, Z.: Development Trends and Prospects of Semiconductor Devices and Technology. Highlights Sci. Eng. Technol. **81**, 374–380 (2024)
4. Kuznetsova, L.S., Arlyapov, V.A., Kamanina, O.A., Lantsova, E.A., Tarasov, S.E., Reshetilov, A.N.: Development of Nanocomposite Materials Based on Conductive Polymers for Using in Glucose Biosensor. Polymers (Basel). **14**, 1543 (2022)
5. Goci, M.C., Leudjo Taka, A., Martin, L., Klink, M.J.: Chitosan-Based Polymer Nanocomposites for Environmental Remediation of Mercury Pollution. Polymers (Basel). **15**, 482 (2023)
6. Ibrahim, A., Klopocinska, A., Horvat, K., Abdel Hamid, Z.: Graphene-Based Nanocomposites: Synthesis, Mechanical Properties, and Characterizations. Polymers (Basel). **13**, 2869 (2021)
7. AL-Maqate, F.G., Qasem, A., Alomayri, T., Madani, A., Timoumi, A., Hussain, D., Ikram, M., Al-Malki, K.M., Bruno, T.A.: Profundity study on structural and optical properties of heavy oil fly ash (HOFA) doped calcium carbonate (CaCO3) nanostructures

and thin films for optoelectronic applications. Opt. Mater. (Amst). **131**, 112719 (2022)
8. Hakamy, A.: Effect of $CaCO_3$ nanoparticles on the microstructure and fracture toughness of ceramic nanocomposites. J. Taibah Univ. Sci. **14**, 1201–1207 (2020)
9. Romero-Fierro, D., Bustamante-Torres, M., Bravo-Plascencia, F., Magaña, H., Bucio, E.: Polymer-Magnetic Semiconductor Nanocomposites for Industrial Electronic Applications. Polymers (Basel). **14**, 2467 (2022)
10. Li, Z., Yang, H., Zhang, D., Zhou, W., Gao, N., Wang, J., Yang, D.: Effects of Bi and S co-doping on the enhanced photoelectric performance of ZnO: Theoretical and experimental investigations. J. Alloys Compd. **872**, 159648 (2021)
11. Liao, X., Wang, X., Huang, C., Zhu, L.: Copper- and Nitrogen-Codoped Graphene with Versatile Catalytic Performances for Fenton-Like Reactions and Oxygen Reduction Reaction. Catalysts. **10**, 1326 (2020)
12. Li, Y., Wang, S., Chang, W., Zhang, L., Wu, Z., Song, S., Xing, Y.: Preparation and enhanced photocatalytic performance of sulfur doped terminal-methylated g-C 3 N 4 nanosheets with extended visible-light response. J. Mater. Chem. A. **7**, 20640–20648 (2019)
13. Ayyakannu Sundaram, G., Kanniah, R., Karthikeyan, V.: Tuning the Magnetic and Photocatalytic Properties of Wide Bandgap Metal Oxide Semiconductors for Environmental Remediation. In: Updates on Titanium Dioxide. IntechOpen (2023)
14. Yu, J., Zheng, Z., Wang, A., Humayun, M., Attia, Y.A.: MoO_3 with the Synergistic Effect of Sulfur Doping and Oxygen Vacancies: The Influence of S Doping on the Structure, Morphology, and Optoelectronic Properties. Nanomaterials. **14**, 1189 (2024). https://doi.org/10.3390/nano14141189
15. Habte, L., Shiferaw, N., Mulatu, D., Thenepalli, T., Chilakala, R., Ahn, J.: Synthesis of Nano-Calcium Oxide from Waste Eggshell by Sol-Gel Method. Sustainability. **11**, 3196 (2019). https://doi.org/10.3390/su11113196.
16. Cheng, H., Wei, J., Liang, M., Dai, S., Liu, X., Ma, L., Wang, H., Lai, F.: Calcium Glycerolate Catalyst Derived from Eggshell Waste for Cyclopentadecanolide Synthesis. Front. Chem. **9**, (2021)
17. Manoharan, K., Krishna Chandar, N.R.: Hydrothermal Synthesis and Characterization of Sulfur-doped g-C3N4/VS4 nanocomposite for efficient photocatalytic applications. Inorg. Chem. Commun. **155**, 111047 (2023)
18. Malata, G., Tkaczewska, E.: Application of thermal methods in the studies of potential pozzolanic reactivity of attapulgite and sepiolite. J. Therm. Anal. Calorim. **148**, 7611–7622 (2023)
19. Khachani, M., El Hamidi, A., Halim, M., Arsalane, S.: Non-isothermal kinetic and thermodynamic studies of the dehydroxylation process of synthetic calcium hydroxide Ca(OH) 2. J. Mater. Environ. Sci. **5**, 615–624 (2014)
20. Naik, T.S.S.K., Singh, S., Narasimhappa, P., Varshney, R., Singh, J., Khan, N.A., Zahmatkesh, S., Ramamurthy, P.C., Shehata, N., Kiran, G.N., Sunil, K.: Green and sustainable synthesis of CaO nanoparticles: Its solicitation as a sensor material and electrochemical detection of urea. Sci. Rep. **13**, 19995 (2023)
21. Dai, F., Zhuang, Q., Huang, G., Deng, H., Zhang, X.: Infrared Spectrum Characteristics and Quantification of OH Groups in Coal. ACS Omega. **8**, 17064–17076 (2023)
22. Roy, K., Debnath, S.C., Raengthon, N., Potiyaraj, P.: Understanding the reinforcing efficiency of waste eggshell-derived nano calcium carbonate in natural rubber composites with maleated natural rubber as compatibilizer. Polym. Eng. Sci. **59**, 1428–1436 (2019)
23. Dhewang, I.B., Yudiati, E., Subagiyo, S., Alghazeer, R.: Carrageenan Extraction of Kappaphycus alvarezii Seaweed from Nusa Lembongan Waters Using Different Alkaline

Treatments. J. Kelaut. Trop. **26**, 238–244 (2023)
24. Thongboon, S., Chukeaw, T., Niamnuy, C., Roddecha, S., Prapainainar, P., Chareonpanich, M., Kingwascharapong, P., Faungnawakij, K., Rupprechter, G., Seubsai, A.: Pineapple-Leaf-Derived, Copper-PAN-Modified Regenerated Cellulose Sheet Used as a Hydrogen Sulfide Indicator. ACS Omega. **8**, 17134–17142 (2023)
25. Vinayan, B.P., Zhao-Karger, Z., Diemant, T., Chakravadhanula, V.S.K., Schwarzburger, N.I., Cambaz, M.A., Behm, R.J., Kübel, C., Fichtner, M.: Performance study of magnesium–sulfur battery using a graphene based sulfur composite cathode electrode and a non-nucleophilic Mg electrolyte. Nanoscale. **8**, 3296–3306 (2016)
26. Koczoń, P., Hołaj-Krzak, J.T., Palani, B.K., Bolewski, T., Dąbrowski, J., Bartyzel, B.J., Gruczyńska-Sękowska, E.: The Analytical Possibilities of FT-IR Spectroscopy Powered by Vibrating Molecules. Int. J. Mol. Sci. **24**, 1013 (2023)
27. Nandiyanto, A.B.D., Oktiani, R., Ragadhita, R.: How to Read and Interpret FTIR Spectroscope of Organic Material. Indones. J. Sci. Technol. 4, 97 (2019).
28. Jayaprabakar, J., Karthikeyan, A., Vijai Anand, K., Arunkumar, T., Anbazhaghan, N., Rangasamy, G.: Synthesis and characterization of calcium oxide nano particles obtained from biowaste and its combustion characteristics in a biodiesel operated compression ignition engine. Fuel. **350**, 128839 (2023)
29. Putz, H.: MATCH!-Phase Analysis Using Powder Diffraction, (2022)
30. OriginLab: Version 95E. OriginLab Corporation, www.OriginLab.com, (2018)
31. Fiquet, G., Richet, P., Montagnac, G.: High-temperature thermal expansion of lime, periclase, corundum and spinel. Phys. Chem. Miner. **27**, 103–111 (1999)
32. Kamhi, S.R.: On the structure of vaterite $CaCO_3$. Acta Crystallogr. 16, 770–772 (1963)
33. Crichton, W.A., Vaughan, G.B.M., Mezouar, M.: In situ structure solution of helical sulphur at 3GPa and 400ºC. Zeitschrift für Krist. - Cryst. Mater. **216**, 417–419 (2001)
34. Aga, K.W., Efa, M.T., Beyene, T.T.: Effects of Sulfur Doping and Temperature on the Energy Bandgap of ZnO Nanoparticles and Their Antibacterial Activities. ACS Omega. **7**, 10796–10803 (2022)
35. Xie, X.-Y., Zhan, P., Li, L.-Y., Zhou, D.-J., Guo, D.-Y., Meng, J.-X., Bai, Y., Zheng, W.-J.: Synthesis of S-doped ZnO by the interaction of sulfur with zinc salt in PEG200. J. Alloys Compd. **644**, 383–389 (2015)
36. Hunter, B.: Rietica for Window, https://www.rietica.com, (2016)
37. Kisi, E.H.: Rietveld analysis of powder diffraction patterns. In: Materials Forum (1994)
38. Hussein, A.M., Dannoun, E.M.A., Aziz, S.B., Brza, M.A., Abdulwahid, R.T., Hussen, S.A., Rostam, S., Mustafa, D.M.T., Muhammad, D.S.: Steps Toward the Band Gap Identification in Polystyrene Based Solid Polymer Nanocomposites Integrated with Tin Titanate Nanoparticles. Polymers (Basel). **12**, 2320 (2020)
39. Morab, S., Sundaram, M.M., Pivrikas, A.: Review on Charge Carrier Transport in Inorganic and Organic Semiconductors. Coatings. **13**, 1657 (2023)